

Electronic Supplementary Information

Abnormal Room Temperature Phosphorescence of Purely Organic Boron-Containing Compounds: the Relationship between the Emissive Behavior and the Molecular Packing, and the Potential Related Applications

Zhaofei Chai,^a Can Wang,^a Jinfeng Wang,^a Fan Liu,^a Yujun Xie,^a Yong-Zheng Zhang,^b Jian-Rong Li,^b Qianqian Li^a and Zhen Li^{*a}

^a Department of Chemistry, Hubei Key Lab on Organic and Polymeric Opto-Electronic Materials, Wuhan University, Wuhan 430072, China.

^b Department of Chemistry and Chemical Engineering, Beijing University of Technology, Beijing 100124, China.

Content

1. Additional background information (Fig. S1-S3)	2
2. Additional spectral information and molecular alignment of PBA-AlkO (Fig. S4-S13, Table S1, S2)	6
3. Frontier orbitals and $S_1 \rightarrow T_n$ transition configurations of PBA-MeO (Fig. S14, S15, Table S3)	12
4. Emission properties of PBA-Xs and tPBA-Xs and tPBA-AlkOs (Fig. S16-S18)	17
5. Additional analysis of single-crystal data or XRD patterns (PBA, PBA-Br, PBA-I, tPBA-MeO, tPBA-F, tPBA-Br, Fig. S19-S28)	19
6. Summary of single-crystal data (Table S4, S5)	24
7. Compound survey (Fig. S29-S40)	26
8. Enlarged drawing and fluorescence photos of crystals through fast crystallization (Fig. S41, S42)	32
9. Patterns of handwriting and inject printing (Fig. S43, S44)	33
10. Results of bio-toxicity determination (Fig. S45, Table S6)	34
11. Materials	35
12. Methods	36
13. Reference	36

1. Additional background information (Fig. S1-S3)

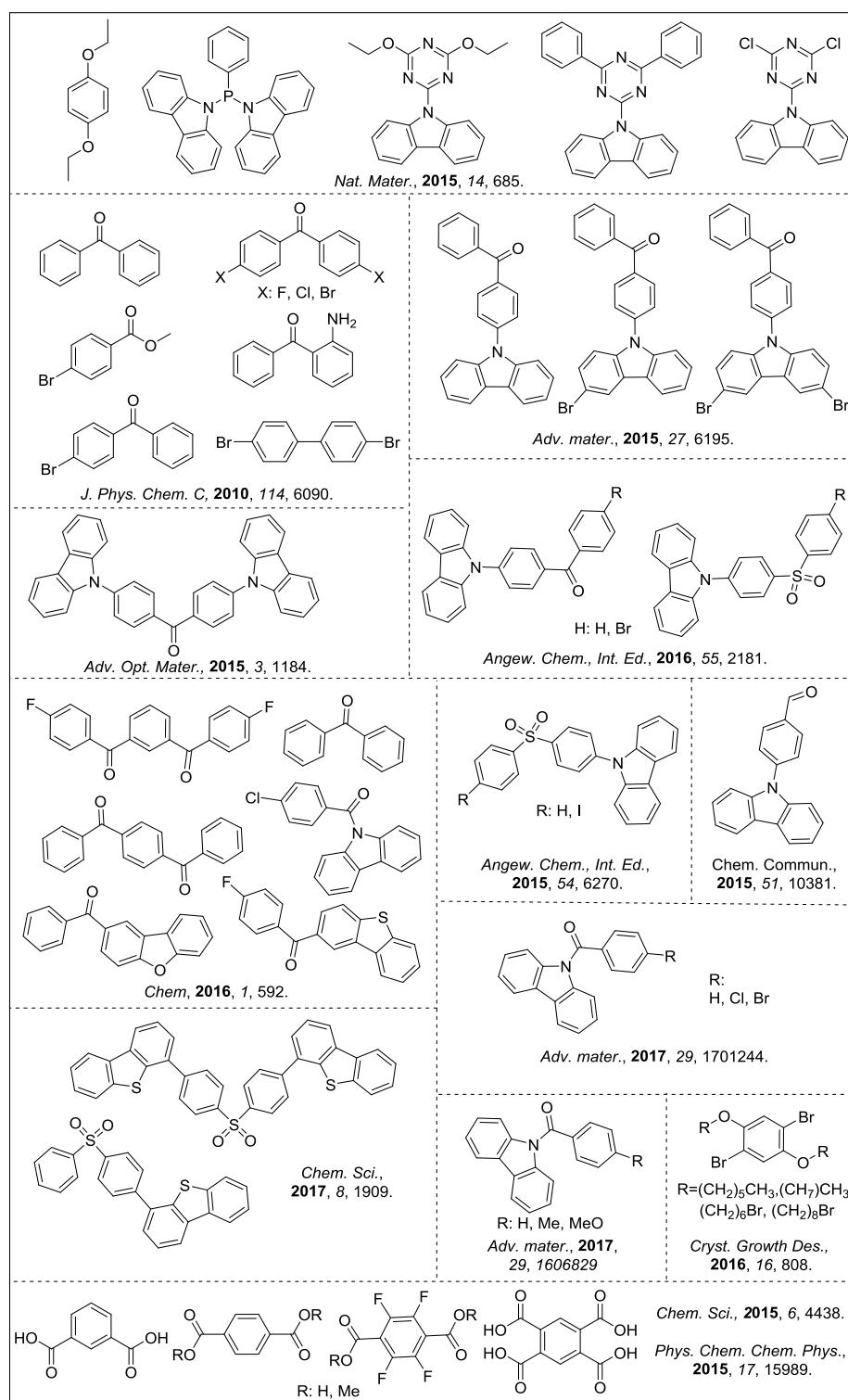


Fig. S1 Typical examples of purely organic phosphors with room-temperature phosphorescence (RTP) properties.

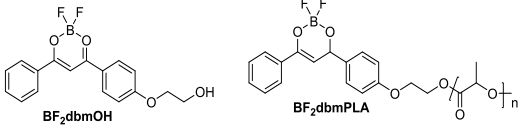
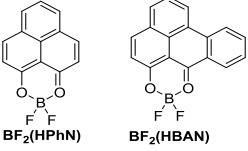
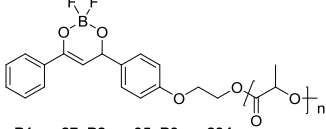
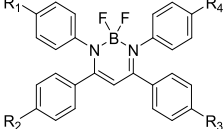
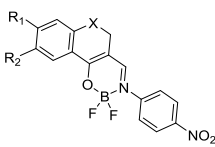
 <p>BF₂dbmOH does not show any detectable RTP; BF₂dbmPLA showed RTP with a lifetime of 0.17 s in the absence of O₂. [S1]</p>	 <p>BF₂(HPhN) and BF₂(HBAN) in polystyrene showed RTP with a lifetime of 360 and 730 ms, respectively. [S2]</p>																																
 <p>P1: n=27 P2: n=95 P3: n=234</p> <p>P1, P2 and P3 showed RTP with lifetimes of 4.06, 4.39, 4.50 ms, respectively in nitrogen. [S3]</p>	 <p>Boron Diiminate Derivatives</p> <p>AIE and CIEE-active boron diiminate derivatives showed phosphorescence at -77 K, but not at ambient conditions. [S4]</p>																																
 <table border="1" data-bbox="550 907 742 1064"> <thead> <tr> <th></th> <th>X</th> <th>R₁</th> <th>R₂</th> </tr> </thead> <tbody> <tr> <td>1</td> <td>CH₂</td> <td>H</td> <td>H</td> </tr> <tr> <td>2</td> <td>CH₂</td> <td>F</td> <td>H</td> </tr> <tr> <td>3</td> <td>CH₂</td> <td>OCH₃</td> <td>H</td> </tr> <tr> <td>4</td> <td>O</td> <td>H</td> <td>H</td> </tr> <tr> <td>5</td> <td>O</td> <td>F</td> <td>H</td> </tr> <tr> <td>6</td> <td>O</td> <td>H</td> <td>OCH₃</td> </tr> <tr> <td>7</td> <td>O</td> <td>H</td> <td>CH₃</td> </tr> </tbody> </table> <p>Compound 1-7 showed short-lived RTP in solutions (< 5.4 μs). While, RTP lifetimes were not given in neat solid or in doped PMMA thin films. [S5]</p>		X	R ₁	R ₂	1	CH ₂	H	H	2	CH ₂	F	H	3	CH ₂	OCH ₃	H	4	O	H	H	5	O	F	H	6	O	H	OCH ₃	7	O	H	CH ₃	<p>[S1] <i>J. Am. Chem. Soc.</i>, 2007, <i>129</i>, 8942.</p> <p>[S2] <i>Nat. Commun.</i>, 2014, <i>5</i>, 4460.</p> <p>[S3] <i>Nat. Mater.</i>, 2009, <i>8</i>, 747.</p> <p>[S4] <i>J. Am. Chem. Soc.</i>, 2014, <i>136</i>, 18131.</p> <p>[S5] <i>Angew. Chem. Int. Ed.</i>, 2014, <i>53</i>, 6378.</p>
	X	R ₁	R ₂																														
1	CH ₂	H	H																														
2	CH ₂	F	H																														
3	CH ₂	OCH ₃	H																														
4	O	H	H																														
5	O	F	H																														
6	O	H	OCH ₃																														
7	O	H	CH ₃																														

Fig. S2 Typical examples of boron-containing materials with RTP properties.

Hyperfine-coupling-driven intersystem crossing	Out-of-plane distortion at the (pinacol)-B-C _{ipso} moiety in the T ₁ state
<p>X: F, Cl, Br, I</p>	
Hideya <i>et al. ChemPhotoChem</i> 2017 , <i>1</i> (3), 102-106. ¹	Fukushima <i>et al. J. Am. Chem. Soc.</i> 2017 , <i>139</i> (7), 2728-2733. ²
<i>Self-restraint and effective π-π stacking interactions</i>	

Fig. S3. Chemical structures involved in the work reported in literatures and ours. The X-ray

single-crystal diffraction data of green ones were obtained by ourselves or adapted from Cambridge Structural Database. RTP of compounds with pink numbers could be observed by naked eyes.

2. Additional spectral information and molecular alignment of PBA-AlkO (Fig. S4-S12, Table S1, S2)

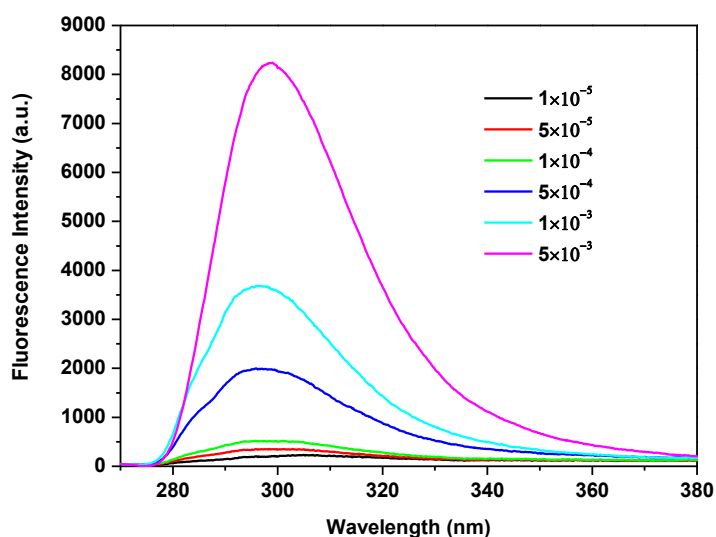


Fig. S4 Fluorescence spectra of PBA-MeO in MeOH at different concentrations ($\lambda_{\text{ex}} = 254$ nm, room temperature, under ambient conditions).

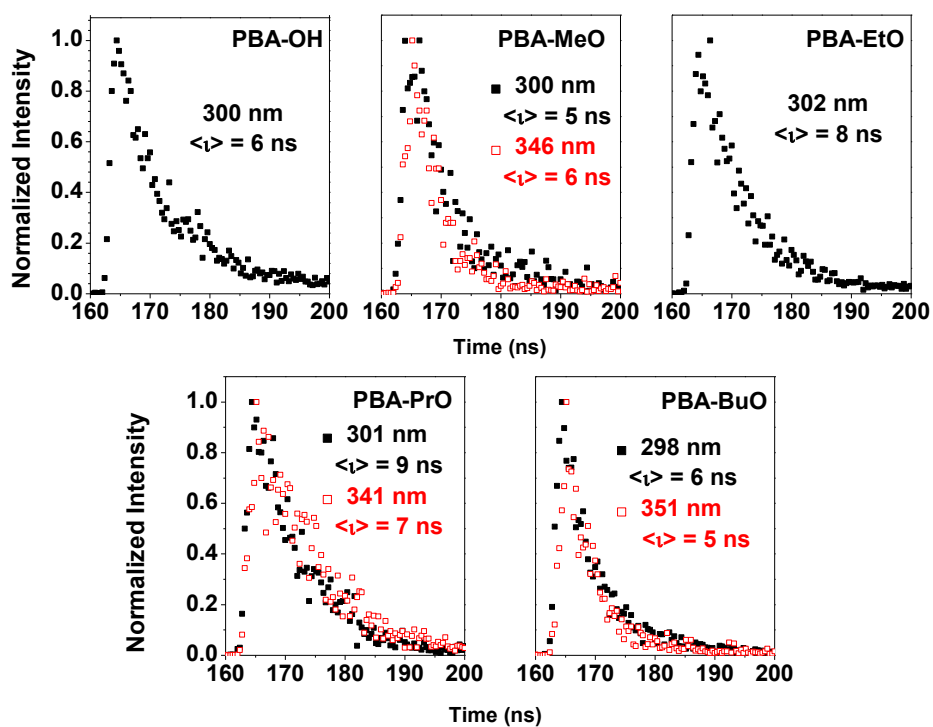


Fig. S5 Fluorescence decay profiles of PBA-AlkO in crystalline states.

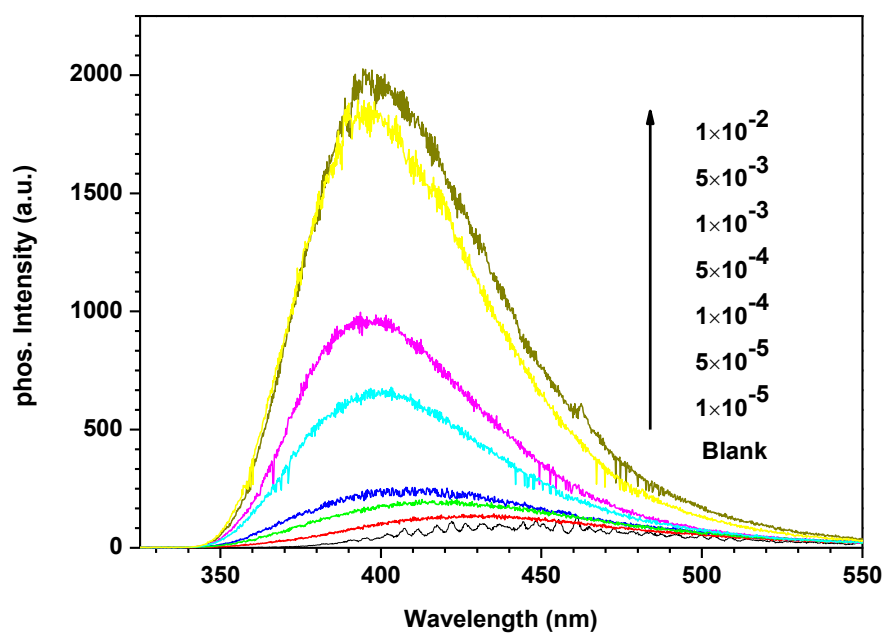


Fig. S6 Phosphorescence spectra of PBA-MeO in MeOH at different concentrations ($\lambda_{\text{ex}} = 280$ nm, 77 K, in air).

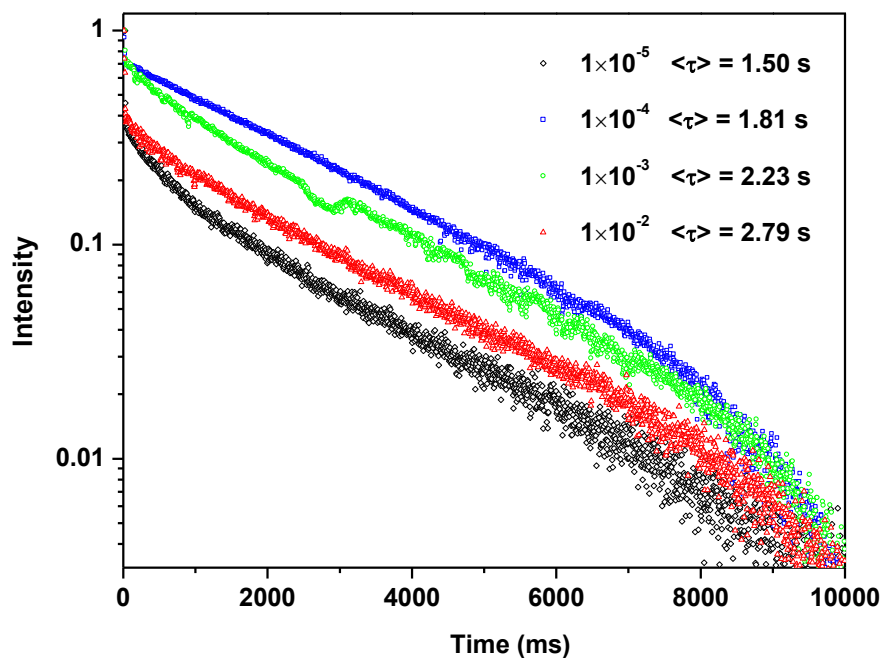


Fig. S7 Phosphorescence decay profiles of PBA-MeO in MeOH at different concentrations ($\lambda_{\text{ex}} = 280$ nm, 77 K, in air).

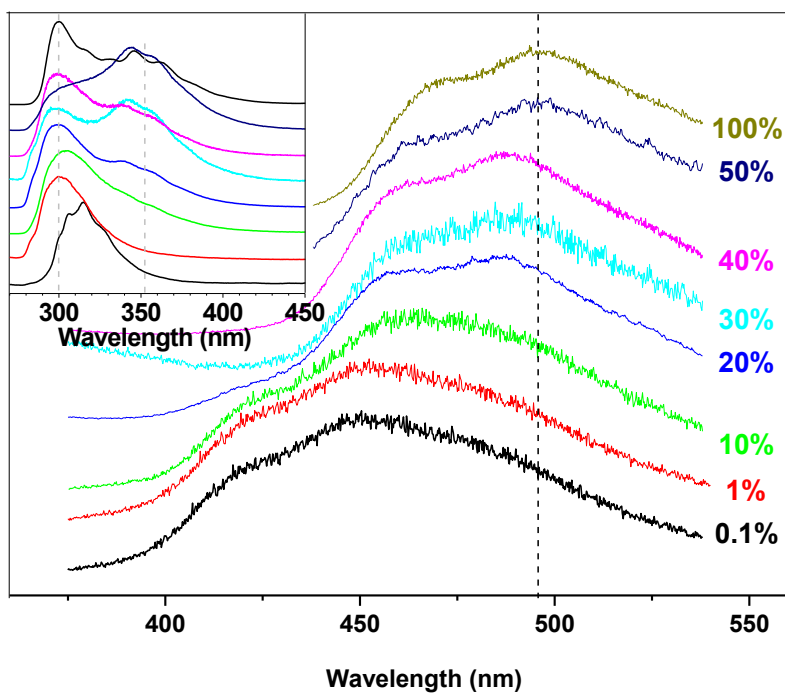


Fig. S8 Phosphorescence spectra of PBA-MeO embedded in PMMA ($\lambda_{\text{ex}} = 280$ nm, room temperature, in air). Inset shows the corresponding fluorescence spectra. When the concentration is higher than 20%, the content of PBA-MeO is too high to form uniform films, which showed irregular changes.

Table S1 RTP properties of PBA-MeO doped in PMMA.

Content (weight %)	0.01	0.1	1	10	20	30 ^b	40 ^b	50 ^b	100 ^c
Wavelength (nm) ^d	443	444	445	468	484	489	487	488	496
Lifetime (ms) ^e	nt ^a	0.79	0.81	0.88	2.6	10	402	608	2190

^aNot detected for its weak RTP, ^bThe content of PBA-MeO is too high to form uniform films; ^cPrepared by slow evaporation of PBA-MeO solution at rt; ^dMaximum RTP Wavelength; ^eThe excitation wavelength was 280 nm, and lifetime was monitored by their maximum emission wavelengths.

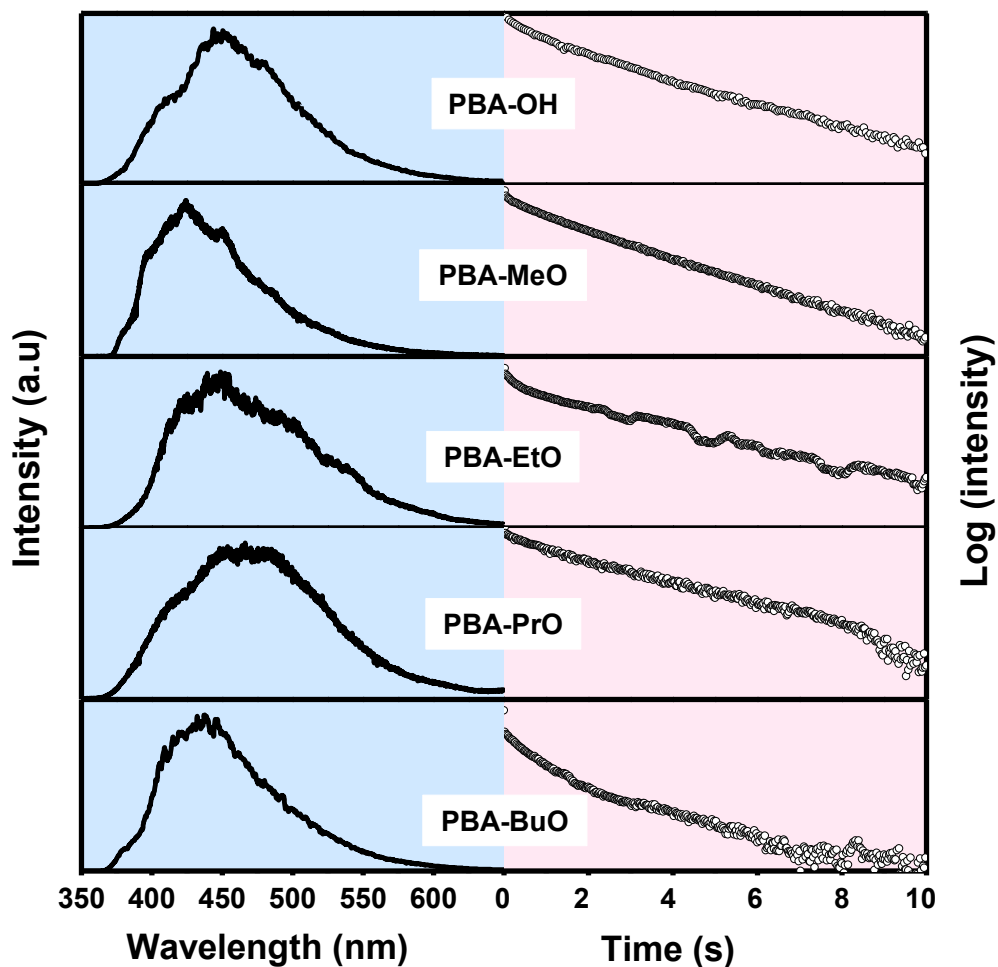


Fig. S9 Phosphorescence spectra ($\lambda_{\text{ex}} = 280$ nm, 77 K, in air) and decay profiles (detected at their maximum emission wavelengths) of PBA-Oalk crystals at 77 K

Table S2 Phosphorescence properties of PBA-Oalk crystals at 298 K and 77 K.

Name	PBA-OH	PBA-MeO	PBA-EtO	PBA-PrO	PBA-BuO
$\lambda_{\text{ex, 298 K}}$ (nm)	291	295	290	290	291
$\lambda_{\text{em, 298 K}}^{\text{max}}$ (nm)	483	488	506	493	492
$\langle \tau \rangle_{\text{Phos. 298 K}}$ (s)	0.713	2.24	1.11	0.129	1.28
$\lambda_{\text{ex, 77 K}}$ (nm)	300				
$\lambda_{\text{em, 77 K}}^{\text{max}}$ (nm)	448	425	450	468	440
$\langle \tau \rangle_{\text{Phos. 77 K}}$ (s)	1.043	1.50	1.070	1.572	0.459

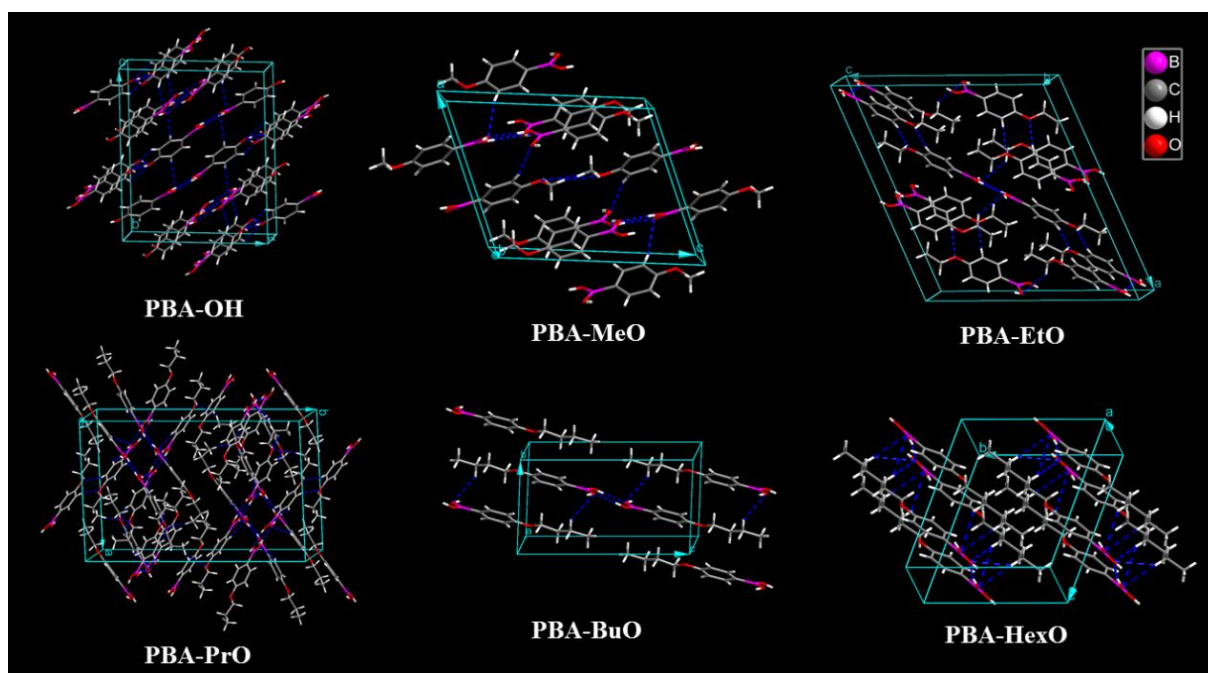


Fig. S10 Unit cells of PBA-OAlks (PBA-OH, PBA-MeO, PBA-EtO, PBA-PrO, PBA-BuO and PBA-HexO). Blue dotted lines represent H-bonds. CH... π or π - π interactions also exist but are not shown for clarity.

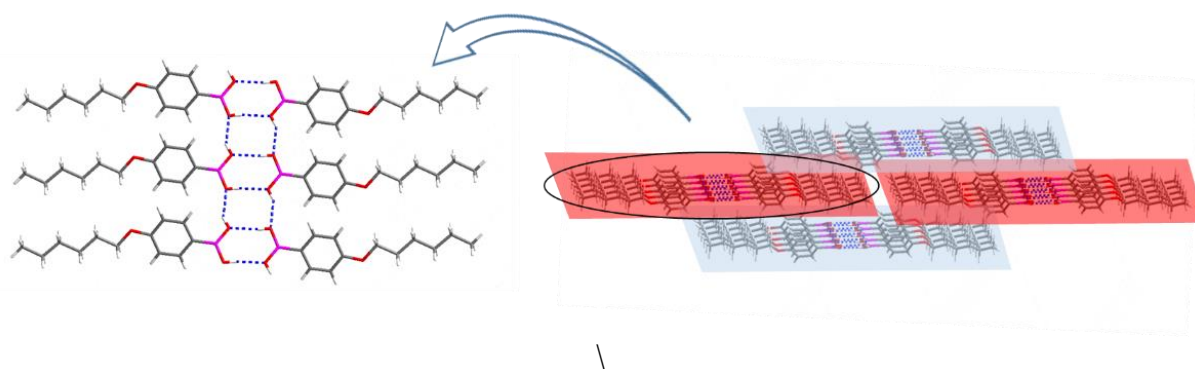


Fig. S11 Diagram of nanoribbons in PBA-HexO single crystals.

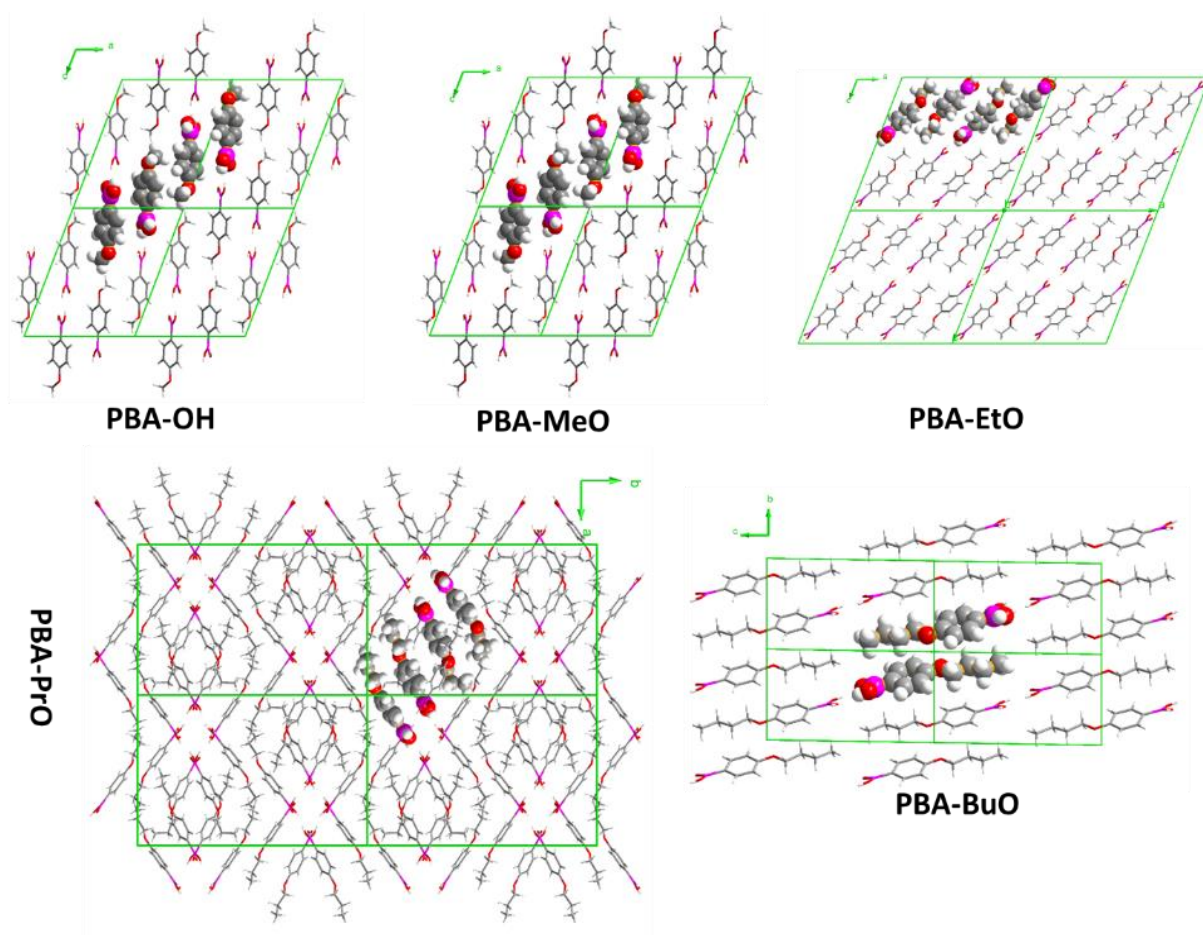


Fig. S12 Diagram of repeating units in Plane 2 ($2 \times 2 \times 2$).

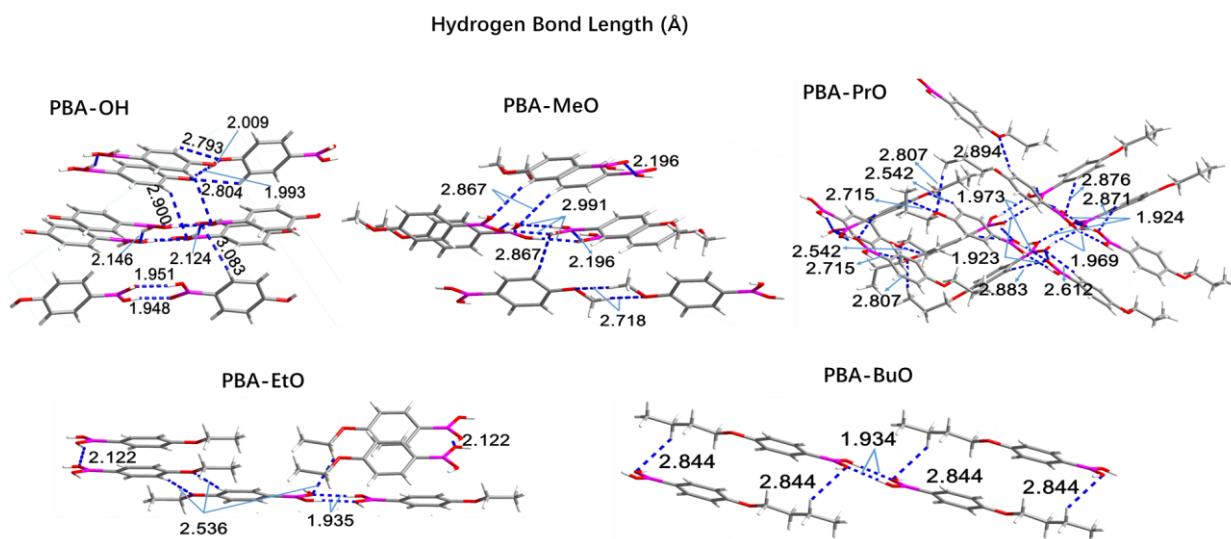


Fig. S13 Hydrogen bond lengths of PBA-Oalks.

3. Frontier orbitals and $S_1 \rightarrow T_n$ transition configurations of PBA-MeO (Fig. S13, Table S3)

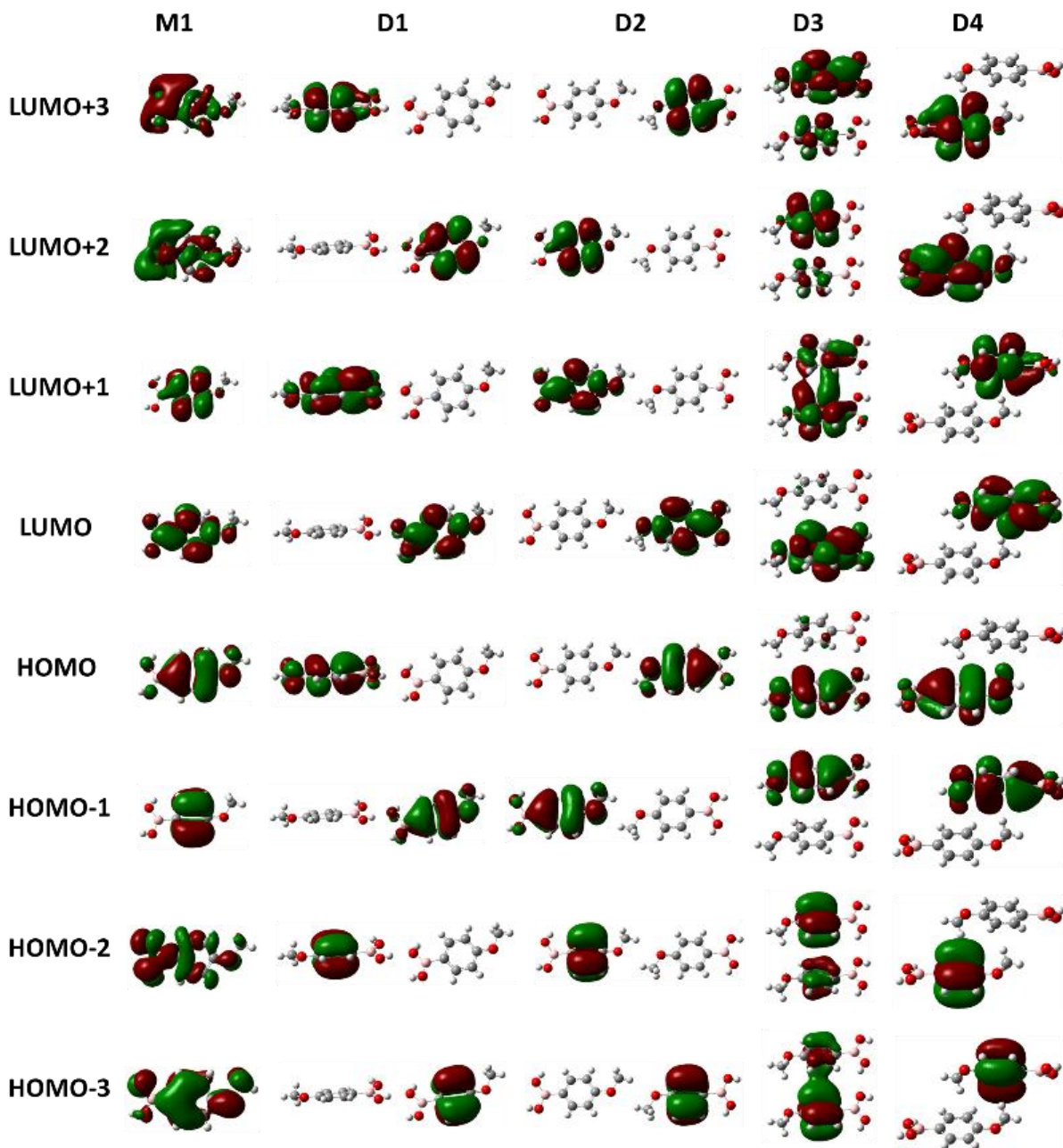
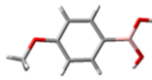
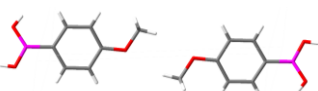


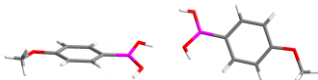
Fig. S14 Frontier orbitals of PBA-MeO monomer and different dimers.

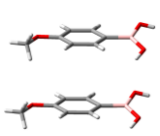
Table S3 The singlet and triplet excited state transition configurations of PBA-MeO monomer and different dimers performed by TD-DFT calculations at the B3LYP/6-31G(d) basis set. The same orbital transition components between S1 and T_n were marked in green.

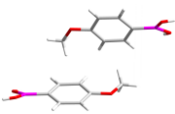
Monomer			
			
n-th	n	Energy (eV)	Transition configuration (%)
S _n	1	5.1392	H-1→L (0.2975), H→L (0.0853), H→L+1 (0.5955)
T _n	1	3.6655	H-1→L+1 (0.2008), H→L (0.7428)
	2	4.3759	H-1→L (0.0318), H→L+1 (0.9462)
	3	4.5506	H-1→L (0.0757), H-1→L+1 (0.6947), H→L (0.2247)
	4	4.9948	H-1→L (0.8578), H-1→L+1 (0.0871), H→L+1 (0.0381)
	5	6.6647	H-5→L (0.0213), H-4→L (0.1063), H-2→L (0.8053)
	6	6.7346	H-4→L (0.0587), H-3→L (0.7634), H→L+2 (0.0273), H→L+3 (0.0406), H→L+9 (0.0234)
	7	6.9525	H-8→L+1 (0.0484), H-3→L+1 (0.6245), H-2→L+1 (0.1343), H-1→L+2 (0.0263), H-1→L+3 (0.0446), H-1→L+9 (0.0285)
	8	7.1298	H-4→L (0.7396), H-4→L+3 (0.0205), H-3→L (0.0541), H-2→L (0.1051)
	9	7.2706	H-5→L (0.0409), H-4→L+1 (0.0979), H-3→L (0.0604), H-2→L+1 (0.2382), H→L+2 (0.2134), H→L+3 (0.2683)

P1			
			
n-th	n	Energy (eV)	Transition configuration (%)
S _n	1	5.1430	H-3→L (0.1127), H-2→L+1 (0.1859), H-1→L+1 (0.0519), H-1→L+2 (0.3637), H→L (0.0312), H→L+3 (0.2198)

T _n	1	3.6678	H-2→L+2 (0.2026), H-1→L+1 (0.7309)
	2	4.3835	H-2→L+1 (0.0330), H-1→L+2 (0.9315)
	3	4.3839	H-3→L (0.0331), H→L+3 (0.9317)
	4	4.5534	H-2→L+1 (0.0773), H-2→L+2 (0.6834), H-1→L+1 (0.2243)
	5	4.5540	H-3→L (0.0770), H-3→L+3 (0.6845), H→L (0.2238)
	6	4.9961	H-2→L+1 (0.8469), H-2→L+2 (0.0875), H-1→L+2 (0.0407)
	7	4.9963	H-3→L (0.8472), H-3→L+3 (0.0870), H→L+3 (0.0407)
	8	5.4440	H→L+1 (0.9867)
	9	5.4441	H-1→L (0.9874)

P2			
			
n-th	n	Energy (eV)	Transition configuration (%)
S _n	1	5.1362	H-3→L (0.3097), H-1→L (0.0738), H-1→L+2 (0.5921)
T _n	1	3.6727	H-2→L+1 (0.0218), H-2→L+3 (0.2028), H→L+1 (0.7344)
	2	4.3701	H-2→L+1 (0.0278), H→L+3 (0.9390)
	3	4.3846	H-3→L (0.0368), H-1→L+2 (0.9481)
	4	4.5412	H-3→L (0.0607), H-3→L+2 (0.7152), H-1→L (0.2211)
	5	4.5590	H-2→L+1 (0.0896), H-2→L+3 (0.6745), H→L+1 (0.2259)
	6	4.9602	H-3→L (0.8707), H-3→L+2 (0.0713), H-1→L+2 (0.0403)
	7	5.0240	H-2→L+1 (0.8442), H-2→L+3 (0.1022), H→L+3 (0.0368)
	8	5.2618	H→L (0.9989)
	9	5.6226	H→L+2 (0.9993)

V1 			
n-th	n	Energy (eV)	Transition configuration (%)
S_n	1	4.6857	H→L (0.9880)
T_n	1	3.6644	H-3→L+1 (0.0588), H-2→L+3 (0.1321), H-1→L (0.2371), H→L+1 (0.1374), H→L+2 (0.3629)
	2	4.3302	H-1→L+1 (0.06166), H→L (0.07344), H→L+1 (0.16431), H→L+2 (0.02376), H→L+3 (0.60681)
	3	4.3742	H-3→L (0.0306), H-1→L+1 (0.7439), H-1→L+2 (0.06H-3), H→L+3 (0.0972)
	4	4.4629	H-3→L+1 (0.2218), H-3→L+2 (0.0387), H-3→L+3 (0.0464), H-2→L (0.0311), H-2→L+1 (0.2501), H-2→L+3 (0.11H-3), H-1→L (0.1381), H→L (0.0315), H→L+1 (0.0554), H→L+2 (0.0334)
	5	4.5433	H-3→L (0.0375), H-3→L+1 (0.2339), H-2→L+3 (0.4381), H-1→L (0.0896), H→L+1 (0.0324), H→L+2 (0.1020)
	6	4.7044	H-3→L (0.0284), H-2→L (0.0250), H→L (0.7913), H→L+2 (0.0529), H→L+3 (0.0508)
	7	4.8747	H-3→L (0.4020), H-3→L+2 (0.0201), H-2→L (0.2906), H-2→L+1 (0.0656), H-2→L+2 (0.0609), H-1→L+1 (0.0321), H→L (0.0529), H→L+1 (0.0280)
	8	4.9821	H-3→L (0.1160), H-3→L+1 (0.0598), H-2→L+1 (0.0712), H-2→L+2 (0.5558), H-2→L+3 (0.0436), H-1→L+2 (0.0264), H→L+1 (0.0448), H→L+2 (0.0241)
	9	5.0417	H-2→L+1 (0.0323), H-2→L+2 (0.0407), H-1→L+1 (0.0228), H→L+1 (0.4836), H→L+2 (0.1857), H→L+3 (0.2152)

V2			
			
n-th	n	Energy (eV)	Transition configuration (%)
S _n	1	4.8149	H→L (0.9962)
T _n	1	3.6705	H-3→L (0.0239), H-3→L+1 (0.1899), H-1→L (0.7417)
	2	4.3509	H-2→L+2 (0.0257), H→L+3 (0.9329)
	3	4.3601	H-3→L (0.0253), H-1→L+1 (0.9375)
	4	4.5364	H-2→L+2 (0.0772), H-2→L+3 (0.6922), H→L+2 (0.2126)
	5	4.5503	H-3→L (0.1014), H-3→L+1 (0.6663), H-1→L (0.2184)
	6	4.8153	H→L (0.9884)
	7	4.9830	H-2→L+2 (0.8533), H-2→L+3 (0.0895), H→L+3 (0.0297)
	8	5.0069	H-3→L (0.8049), H-3→L+1 (0.1078), H-1→L+1 (0.0307), H→L+1 (0.0323)
	9	5.0801	H-3→L (0.0241), H→L+1 (0.9404)

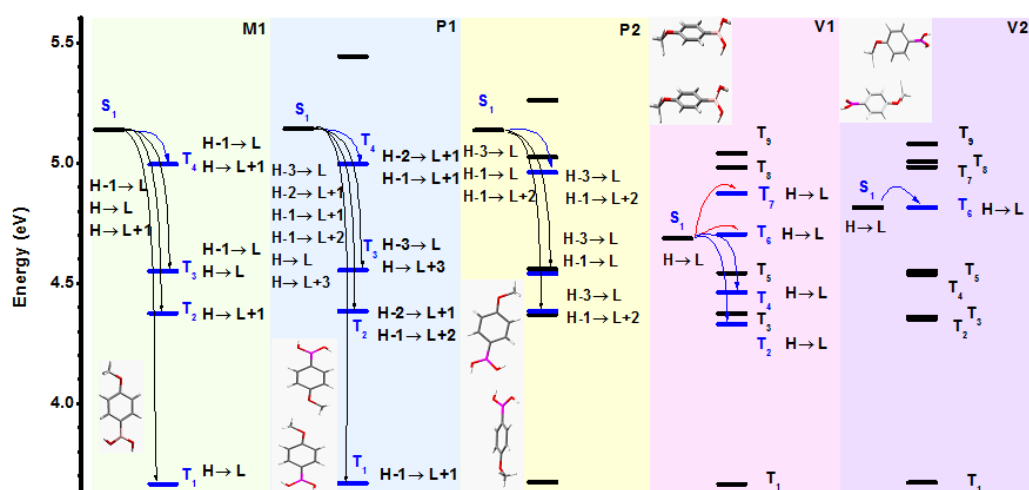


Fig. S15 Schematic diagrams showing the TD-DFT-calculated energy levels at singlet (S₁) and triplet (T_n) states (PBA-MeO). Note that H and L refer to the highest occupied molecular orbital (HOMO) and lowest unoccupied molecular orbital (LUMO), respectively. The blue

arrows represent the probably ISC occurring from the S_1 state to T_n . The dark and red ones refer to the triplet states available but with a larger ΔE_{ST} (0.3 eV).

4. Emission properties of PBA-Xs and tPBA-Xs and tPBA-AlkOs (Fig. S16-S18)

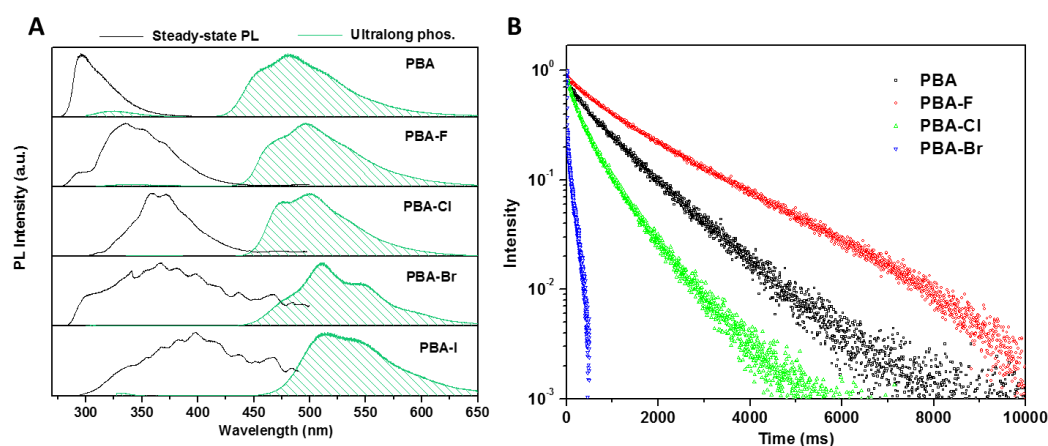


Fig. S16 A: Fluorescence and phosphorescence spectra of the PBA-X crystals. The room temperature fluorescence spectra were recorded at 254 nm, while phosphorescence spectra at their best excitation wavelengths (280-295 nm). B: Room temperature phosphorescence decay profiles excited at their best excitation wavelengths and detected at their maximum emission wavelengths. The RTP intensity of PBA-I was very weak and the lifetime was not determined.

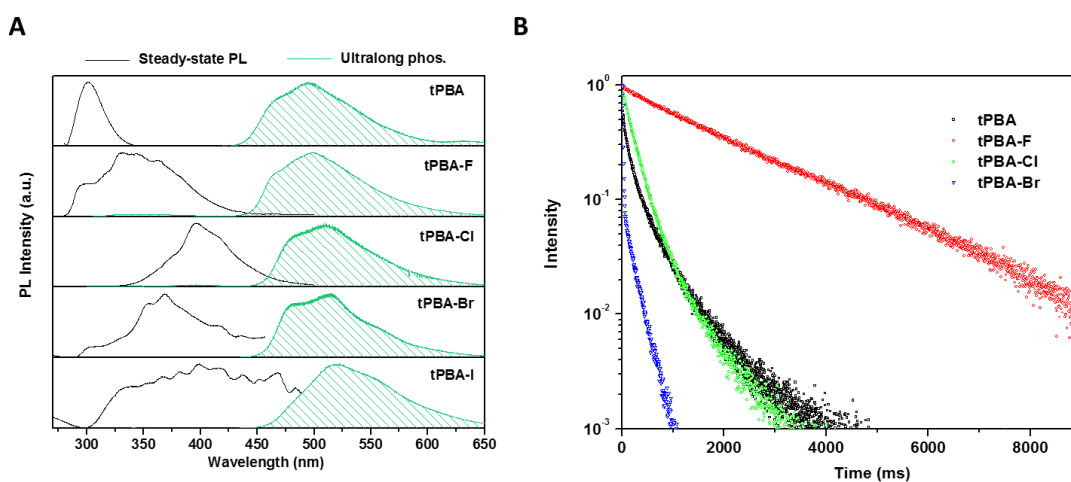


Fig. S17 A: Fluorescence and phosphorescence spectra of the tPBA-X powders. The room temperature fluorescence spectra were recorded at 254 nm, while phosphorescence spectra at

their best excitation wavelengths (280-295 nm). B: Room temperature phosphorescence decay profiles excited at their best excitation wavelengths and detected at their maximum emission wavelengths. The RTP intensity of tPBA-I was very weak and the lifetime was not determined.

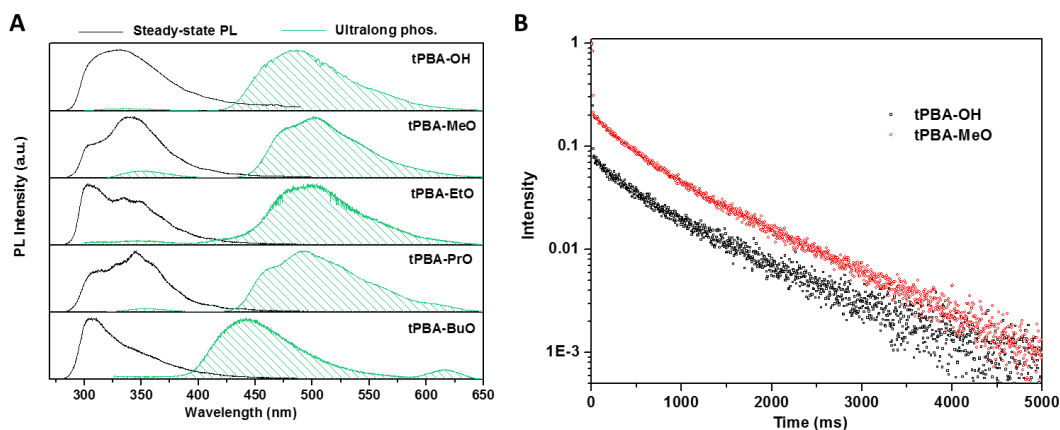


Fig. S18 A: Fluorescence and phosphorescence spectra of the tPBA-AlkO powders. The room temperature fluorescence spectra were recorded at 254 nm, while phosphorescence spectra at their best excitation wavelengths (280-295 nm). B: Room temperature phosphorescence decay profiles excited at their best excitation wavelengths and detected at their maximum emission wavelengths. The RTP intensities of tPBA-EtO, tPBA-PrO and tPBA-BuO were very weak and the lifetimes were not determined.

5. Additional analysis of single-crystal data or XRD patterns (PBA, PBA-Br, PBA-I, tPBA-MeO, tPBA-F, tPBA-Br, Fig. S19-S28)

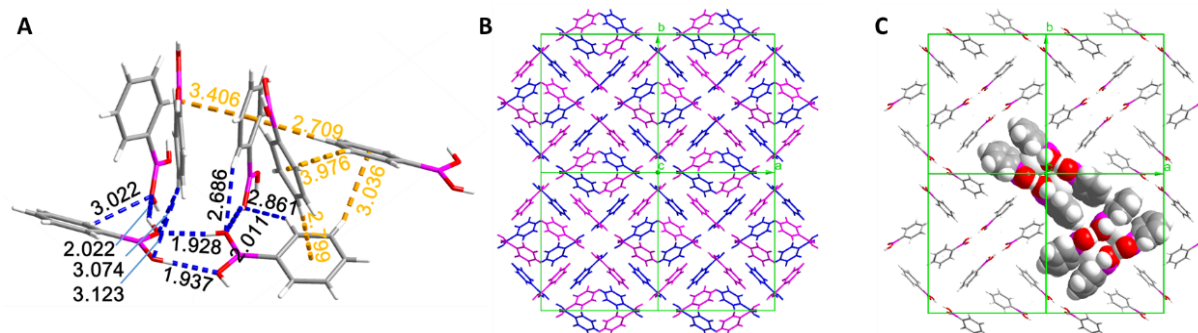


Fig. S19 Packing modes of PBA. A: Bond lengths of different types (H-bonds are marked in blue, while CH... π interactions are in yellow); B: An illustration of two neighbouring layers adopting a herringbone type (Each color represents a different layer); C: Diagram of repeating units. In the absence of *para*-oxygen or alkoxy chains, the molecules are still well restricted. While no long-range π - π stacking interaction was found, which may lead to short-lived lifetime and low RTP intensity compared to that of PBA-OAlks (similar to PBA-PrO).

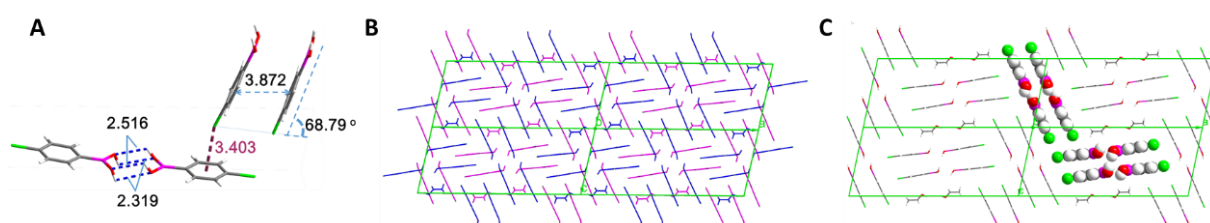


Fig. S20 Packing modes of PBA-Br. A: Bond lengths of different types (Blue and purple dotted lines represent H-bonds and halogen bonds, respectively.); B: An illustration of two neighbouring layers adopting a herringbone type; C: Diagram of repeating units. (CCDC: 263708)³

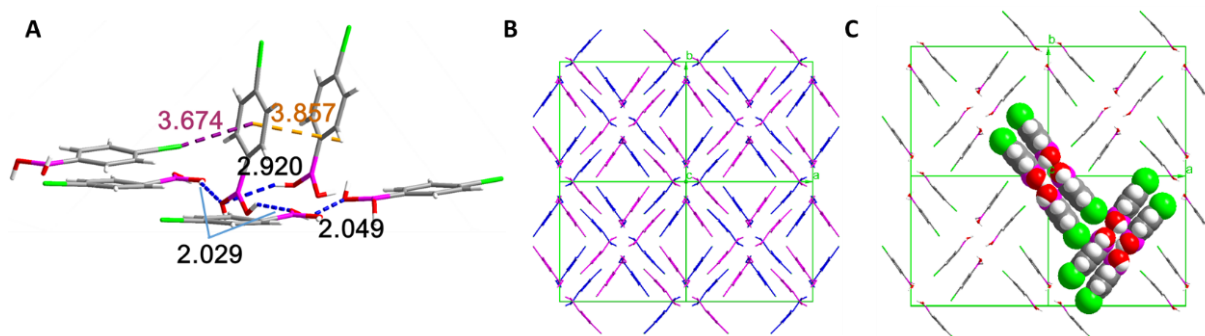


Fig. S21 Packing modes of PBA-I. A: Bond lengths of different types (Blue, yellow and purple dotted lines represent H-bonds, CH... π interactions and halogen bonds, respectively); B: An illustration of two neighbouring layers adopting a herringbone type; C: Diagram of repeating units. From Fig. S17-19, we can find that the packing modes of PBA, PBA-Br and PBA-I are very similar to each other and adopt a herringbone type. Br and I build halogen bonds, which are longer than that of H-bond for phenylboric acid (*p*-H of PBA), leading to the decrease of interaction and then loose immobilization of molecules. The replacement of H by Br and I also decreases the total number of H-bonds. And the approach of neighbouring Br and I may also accelerate the ISC process and lead to short-lived lifetime.

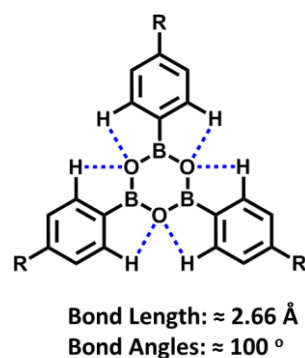


Fig. S22 The illustration of intramolecular hydrogen bonds in boroxine. After dehydration, the oxygen atoms of boroxine are surrounded by aromatic rings and form intramolecular hydrogen bonds, which results in larger distance between two layers due to the decreased layer interactions, leading to limited π - π stacking to stabilize excitons. And without heteroatoms to form extra non-covalent bonds (H-bonds and halogen bonds in our system), the molecules could not be fully immobilized to suppress vibration.



Fig. S23 Packing modes of tPBA. A: An illustration of CH... π interactions; B: Molecules arrangement of Packing 1; C: Molecules arrangement of Packing 2. After dehydration, the oxygen atoms are no longer exposed to the periphery of molecules and cannot build H-bonds, thus only weaker CH... π interactions are there to immobilize molecules. Worse, phenyl rings do not form effective π - π stacking to stabilize the excitons. The two shortcomings lead to dim RTP with short-lived lifetime.

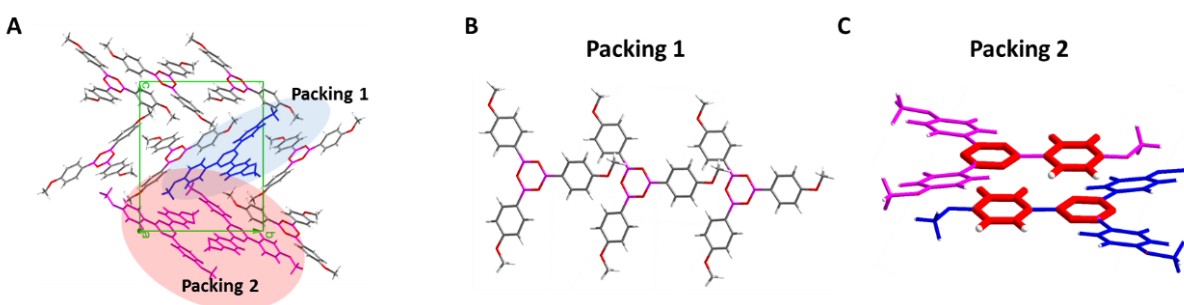


Fig. S24 Packing modes of tPBA-MeO. A: Unit cell of tPBA-MeO. B: Molecules arrangement of Packing 1; C: Molecules arrangement of Packing 2. (The H-bond lengths are limited to 1.9-3.2 Å) (CCDC: 275668)⁴. After dehydration of PBA-MeO, both two-dimensional planes formed by H-bonds and effective π - π stacking of tPBA-MeO have disappeared as shown in Packing 1 and Packing 2. But, the RTP benefits from rigid conformation due to H-bonds built by the MeO- unit (Fig. S20). So, the RTP intensity and lifetime decrease compared to PBA-MeO.

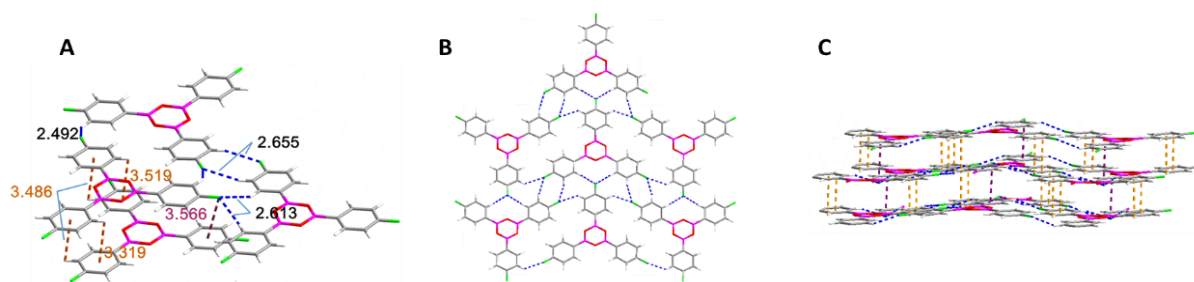


Fig. S25 Packing modes of tPBA-F. A: Bond lengths of different types; B: An illustration of H-bond network in one layer. C: A sketch of non-covalent bonds. (Blue, yellow and purple dotted lines represent H-bonds, CH... π interactions and halogen bonds, respectively.) Due to the presence of fluorine atoms, the packing mode and non-covalent bonds of tPBA-F are very similar to those of PBA-MeO, leading to long-lived RTP.

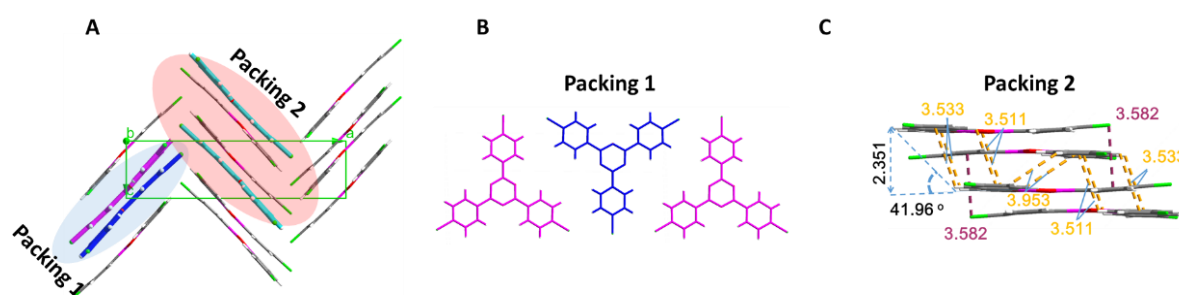


Fig. S26 Packing modes of tPBA-Br. A: Unit cell of tPBA-Br. B: Molecules arrangement of Packing 1; C: Molecules arrangement of Packing 2. (CCDC: 182474)⁵. For tPBA-Br, the π - π stacking is largely enhanced due to the shorter distance of two parallel molecules (3.86 vs 2.35 Å), and the packing mode also decreases the influence of neighbouring Br (3.40 vs 3.58 Å) compared to PBA-Br. So, the RTP was lit up after dehydration of PBA-Br.

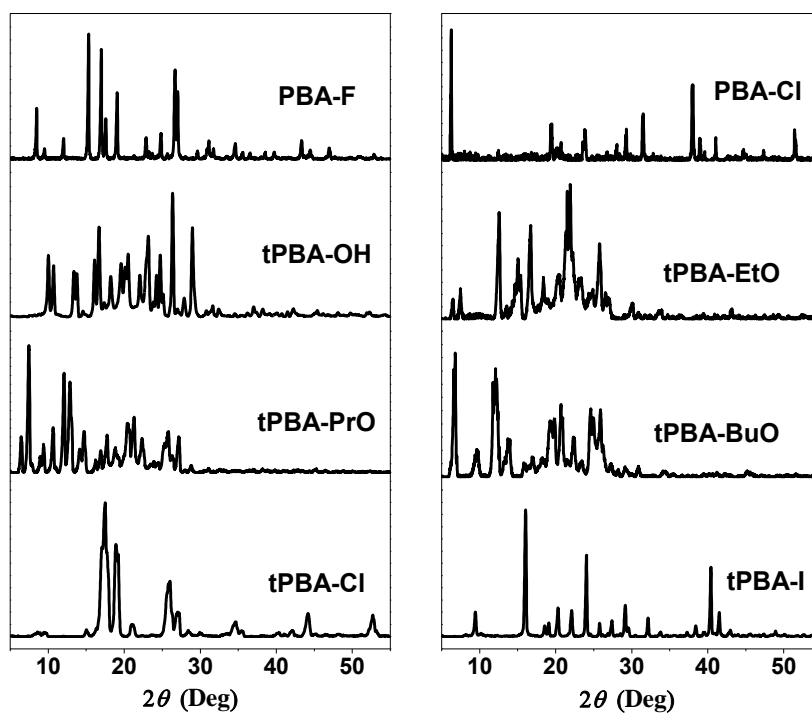


Fig. S27 XRD patterns of PBA-F, PBA-Cl, tPBA-OH, tPBA-EtO, tPBA-PrO, tPBA-BuO, tPBA-Cl and tPBA-I.

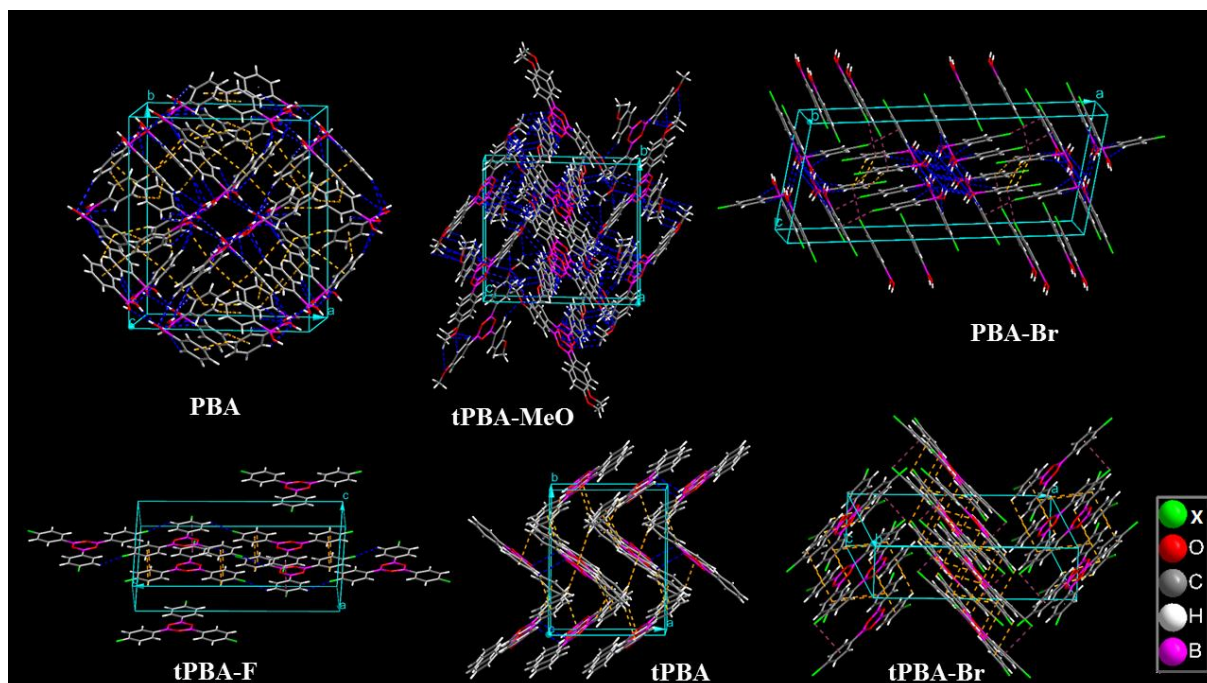


Fig. 28 Unit cells of PBA, tPBA, tPBA-MeO, PBA-Br, tPBA-Br and tPBA-F. Blue, yellow and purple dotted lines represent H-bonds, CH... π interactions and halogen bonds, respectively.

6. Summary of single-crystal data (Table S4, S5)

Table S4 Summary of single-crystal data for PBA-OH, PBA-MeO, PBA-EtO, PBA-PrO and PBA-BuO.

Name	PBA-OH	PBA-MeO	PBA-EtO	PBA-PrO	PBA-BuO
Formula	C ₆ H ₇ BO ₃	C ₇ H ₉ BO ₃	C ₈ H ₁₁ BO ₃	C ₉ H ₁₃ BO ₃	C ₁₀ H ₁₅ BO ₃
Mr	137.93	151.95	165.98	180.00	194.03
Crystal System	Monoclinic	Monoclinic	Monoclinic	Monoclinic	Triclinic
Temperature /K	99.8(4)	296(2)	100.01(10)	296(2)	100.01(10)
Space Group	P2 ₁ /c	P2 ₁ /n	I2/a	P2 ₁ /c	P-1
a /Å	14.3451(6)	11.2586(15)	19.8150(4)	16.193(4)	5.0709(3)
b /Å	5.0353(2)	5.0616(7)	5.02009(8)	24.868(6)	7.6864(7)
c /Å	17.3021(6)	13.8819(18)	18.2337(4)	9.919(2)	13.7993(11)
α /°	90	90	90	90	87.907(7)
β /°	90.473(4)	111.069(2)	111.493(2)	94.666(4)	85.499(6)
γ /°	90	90	90	90	74.195(7)
Volume /Å ³	1249.73(9)	738.20(17)	1687.63(6)	3981.2(15)	515.86(7)
Z	8	4	8	16	2
Density /g cm ⁻³	1.466	1.367	1.307	1.201	1.249
μ /mm ⁻¹	0.114	0.103	0.796	0.087	0.722
F(000)	576.0	320.0	704.0	1536.0	208
Crystal Size	0.3 × 0.3	0.3 × 0.28	0.3 × 0.3	0.3 × 0.2	0.2 × 0.06 ×
/mm ³	× 0.1	× 0.26	× 0.2	× 0.2	0.06
Radiation	0.71073 (Mo-Kα)	0.71073 (Mo-Kα)	1.54184 (Cu-Kα)	0.71073 (Mo-Kα)	1.54184 (Cu-Kα)
h _{max} , k _{max} , l _{max}	18, 6, 23	14, 6, 17	22, 3, 22	20, 31, 12	3, 8, 16
T _{min} , T _{max}	1.00, 0.668	0.970, 0.974	1.00, 0.870	0.979, 0.983	1.00, 0.883
CCDC	1547113	1547361	1547292	1547293	1547294

Table S5 Summary of single-crystal data for PBA-HexO, PBA, PBA-I, tPBA and tPBA-F.

Name	PBA-HexO	PBA	PBA-I	tPBA	tPBA-F
Formula	C ₁₂ H ₁₉ BO ₃	C ₆ H ₇ BO ₂	C ₆ H ₆ BO ₂ I	C ₁₈ H ₁₅ B ₃ O ₃	C ₁₈ H ₁₂ B ₃ F ₃ O ₃
Mr	222.08	121.93	247.82	311.73	365.71
Crystal System	Triclinic	Orthorhombic	Orthorhombic	monoclinic	monoclinic
Temperature /K	296(2)	296(2)	247.82	100.01(10)	100.01(10)
Space Group	P-1	Iba2	Pbcn	P2 ₁ /c	P2 ₁ /m
a /Å	5.0668(13)	15.322(3)	19.5310(10)	10.6824(5)	3.8105(3)
b /Å	10.184(3)	17.902(3)	18.4544(8)	13.2062(7)	20.8028(16)
c /Å	13.252(3)	9.8089(17)	9.7999(8)	11.5423(7)	10.3896(10)
α /°	72.888(4)	90	90	90	90
β /°	84.617(4)	90	90	99.843(6)	96.843(8)
γ /°	75.928(4)	90	90	90	90
Volume /Å ³	633.7(3)	2690.5(8)	3532.2(4)	1604.34(15)	817.71(12)
Z	2	16	1856	4	2
Density /g cm ⁻³	1.164	1.204	1.864	1.291	1.485
μ /mm ⁻¹	0.080	0.086	28.036	0.083	0.119
F(000)	240.0	1024.0	1856	648	372
Crystal Size /mm ³	0.3 × 0.28 × 0.27	0.27 × 0.23 × 0.23	0.1 × 0.1 × 0.1	0.3 × 0.2 × 0.15	0.3 × 0.25 × 0.2
Radiation	0.71073 (Mo-Kα)	0.71073 (Mo-Kα)	1.54184 (Cu-Kα)	0.71073 (Mo-Kα)	0.71073 (Mo-Kα)
h _{max} , k _{max} , l _{max}	6, 12, 16	19,22,12	23, 22, 11	13, 12, 15	5, 27, 14
T _{min} , T _{max}	0.976, 0.979	0.977,0.980	1.000, 0.880	1.000, 0.965	1.000, 0.640
CCDC	1547295	1547338	1547298	1519392	1547297

7. Compound Survey. (Fig. S29-S40)

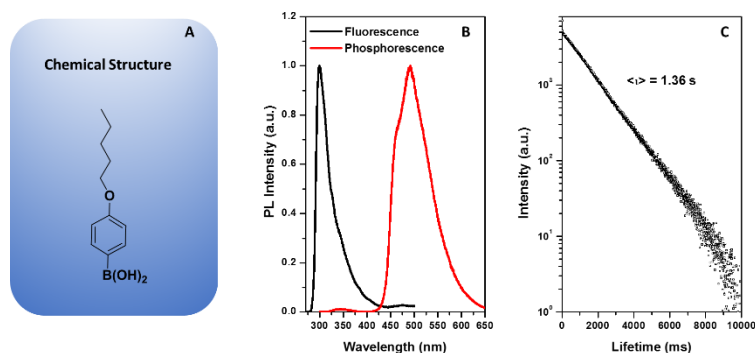


Fig. S29 A: Chemical structure of (4-(pentyloxy)phenyl)boronic acid (PBA-AmO); B: Fluorescence ($\lambda_{ex} = 254$ nm) and phosphorescence ($\lambda_{ex} = 284$ nm) spectra of powder crystals; C: Room temperature phosphorescence decay profiles ($\lambda = 494$ nm) of powder crystals ($\lambda_{ex} = 284$ nm).

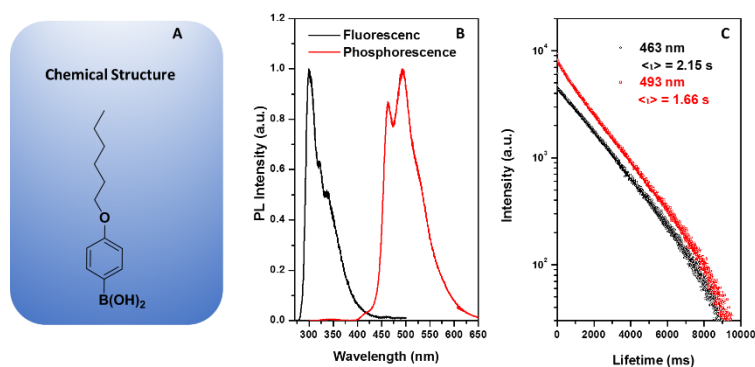


Fig. S30 A: Chemical structure of (4-(hexyloxy)phenyl)boronic acid (PBA-HexO); B: Fluorescence ($\lambda_{ex} = 254$ nm) and phosphorescence ($\lambda_{ex} = 291$ nm) spectra of powder crystals; C: Room temperature phosphorescence decay profiles ($\lambda_{em} = 463$ and 493 nm) of powder crystals ($\lambda_{ex} = 291$ nm).

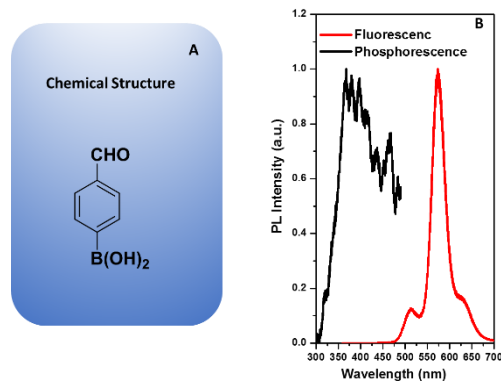


Fig. S31 A: Chemical structure of (4-formylphenyl)boronic acid; B: Fluorescence ($\lambda_{\text{ex}} = 254$ nm) and phosphorescence ($\lambda_{\text{ex}} = 340$ nm) spectra of powder crystals; Room temperature phosphorescence decay profiles was not measured for its short-lived lifetime.

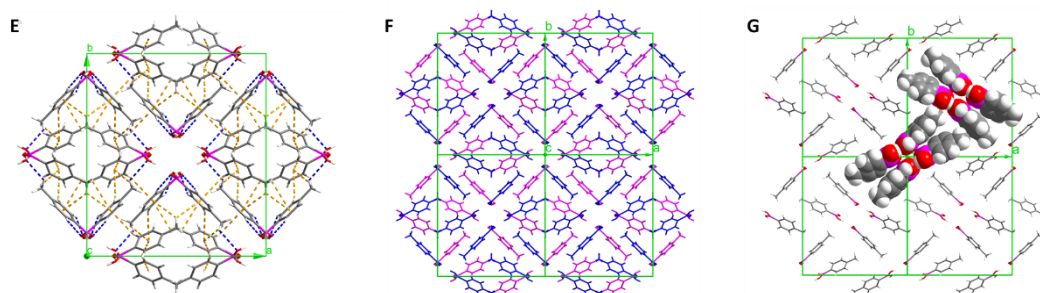
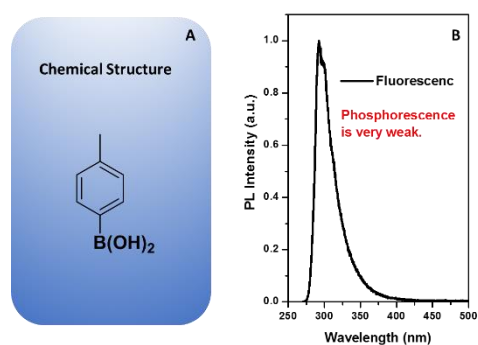


Fig. S32 A: Chemical structure of *p*-tolylboronic acid; B: Fluorescence ($\lambda_{\text{ex}} = 254$ nm) spectrum of powder crystals; Room temperature phosphorescence is too weak to be detected; E: Different types of molecular interactions types (Blue and yellow dotted lines represent H-bonds and CH... π interactions, respectively.); F: An illustration of two neighbouring layers adopting a herringbone type; G: Diagram of repeating units. (CCDC: 186057)

The *p*-methyl group was not well immobilized for the weaker CH... π interactions (>3.0 Å) in comparison with PBA, leading to the quenching of triplet states due to the C-H stretching vibrations. And molecules in one dimer have a twist angle of 28.33° , resulting in the instability of excitons. So *p*-tolylboronic acid is dim before or after UV irradiation.

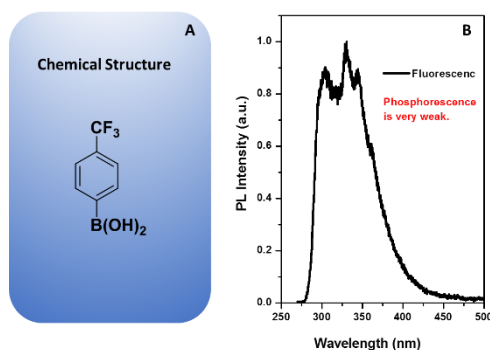


Fig. S33 A: Chemical structure of (4-(trifluoromethyl)phenyl)boronic acid; B: Fluorescence ($\lambda_{\text{ex}} = 254$ nm) spectrum of powder crystals; Room temperature phosphorescence is too weak to be detected.

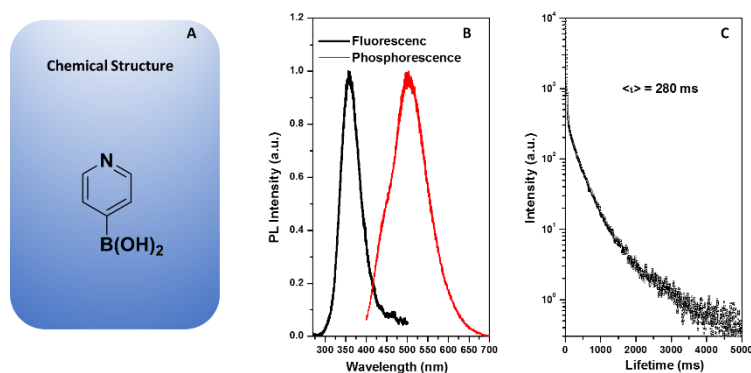


Fig. S34 A: Chemical structure of pyridin-4-ylboronic acid; B: Fluorescence ($\lambda_{\text{ex}} = 254$ nm) and phosphorescence ($\lambda_{\text{ex}} = 370$ nm) spectra of powder crystals; C: Room temperature phosphorescence decay profiles ($\lambda_{\text{em}} = 501$ nm) of powder crystals ($\lambda_{\text{ex}} = 370$ nm).

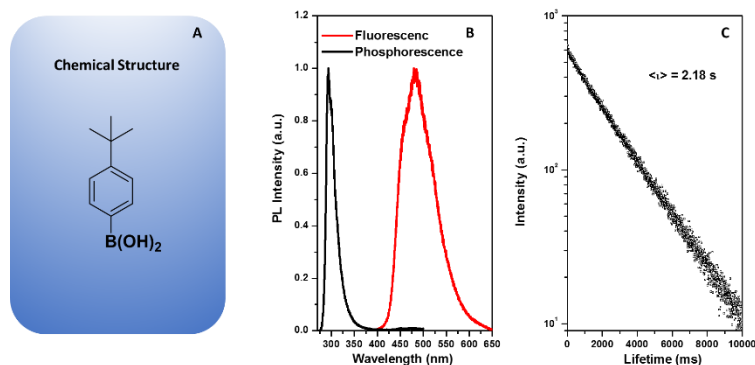


Fig. S35 A: Chemical structure of (4-(tert-butyl)phenyl)boronic acid; B: Fluorescence ($\lambda_{\text{ex}} = 254\text{ nm}$) and phosphorescence ($\lambda_{\text{ex}} = 280\text{ nm}$) spectra of powder crystals; C: Room temperature phosphorescence decay profiles ($\lambda_{\text{em}} = 482\text{ nm}$) of powder crystals ($\lambda_{\text{ex}} = 280\text{ nm}$).

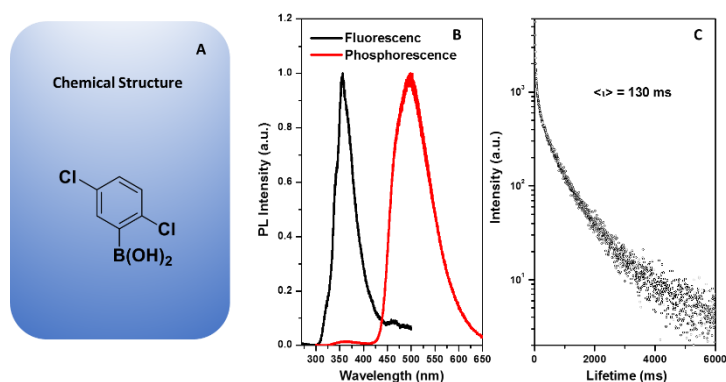


Fig. S36 A: Chemical structure of (2,5-dichlorophenyl)boronic acid; B: Fluorescence ($\lambda_{\text{ex}} = 254\text{ nm}$) and phosphorescence ($\lambda_{\text{ex}} = 284\text{ nm}$) spectra of powder crystals; C: Room temperature phosphorescence decay profiles ($\lambda_{\text{em}} = 495\text{ nm}$) of powder crystals ($\lambda_{\text{ex}} = 284\text{ nm}$).

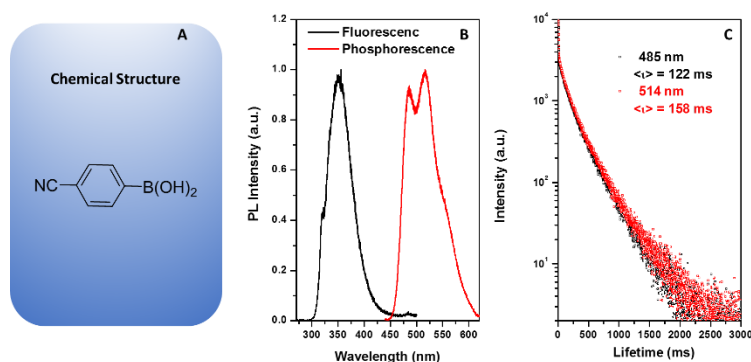


Fig. S37 A: Chemical structure of (4-cyanophenyl)boronic acid (PBA-CN); B: Fluorescence ($\lambda_{\text{ex}} = 254\text{ nm}$) and phosphorescence ($\lambda_{\text{ex}} = 301\text{ nm}$) spectra of powder crystals; C: Room

temperature phosphorescence decay profiles ($\lambda = 485$ and 514 nm) of powder crystals ($\lambda_{\text{ex}} = 301$ nm).

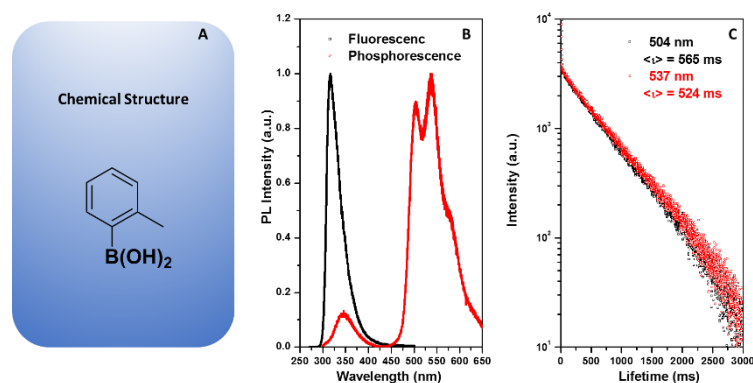


Fig. S38 A: Chemical structure of *o*-tolylboronic acid; B: Fluorescence ($\lambda_{\text{ex}} = 254$ nm) and phosphorescence ($\lambda_{\text{ex}} = 280$ nm) spectra of powder crystals; C: Room temperature phosphorescence decay profiles ($\lambda = 504$ and 537 nm) of powder crystals ($\lambda_{\text{ex}} = 280$ nm).

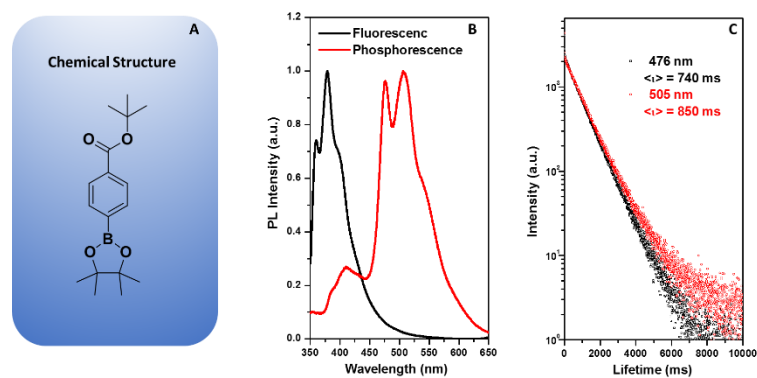


Fig. S39 A: Chemical structure of tert-butyl 4-(4,4,5,5-tetramethyl-1,3,2-dioxaborolan-2-yl)benzoate; B: Fluorescence ($\lambda_{\text{ex}} = 330$ nm) and phosphorescence ($\lambda_{\text{ex}} = 302$ nm) spectra of powder crystals; C: Room temperature phosphorescence decay profiles ($\lambda_{\text{em}} = 476$ and 505 nm) of powder crystals ($\lambda_{\text{ex}} = 302$ nm).

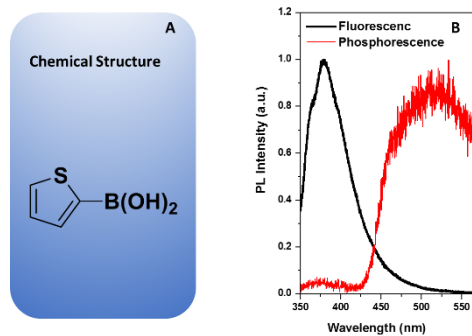


Fig. S40 A: Chemical structure of thiophen-2-ylboronic acid; B: Fluorescence ($\lambda_{\text{ex}} = 254$ nm) and phosphorescence ($\lambda_{\text{ex}} = 294$ nm) spectra of powder crystals; Room temperature phosphorescence is too weak to be detected.

8. Enlarged drawing and fluorescence photos of crystals through fast crystallization.

(Fig. S41 and S42)

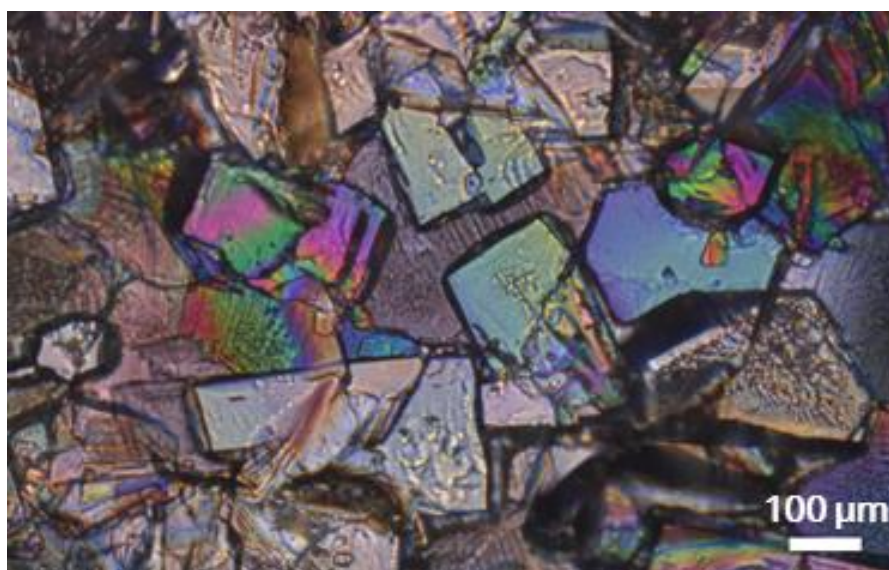


Fig. S41 A partial enlarged drawing of crystals through fast crystallization (bright-field image by a 40x object lens, Olympus IX71).

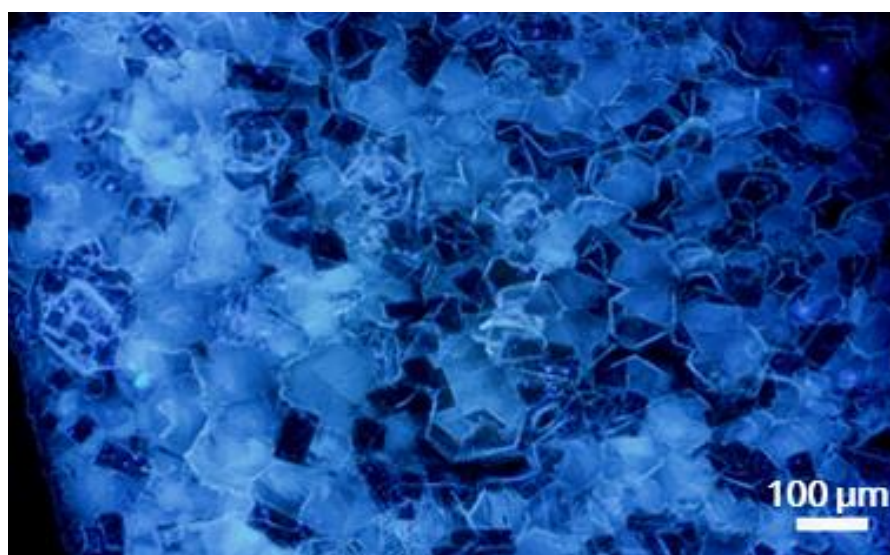


Fig. S42 Fluorescence photos of crystals through fast crystallization (taken on WU channel by a 10x object lens, Olympus IX71).

9. Patterns of handwriting and inject printing. (Fig. S43 and S44)

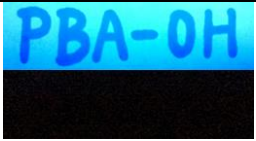








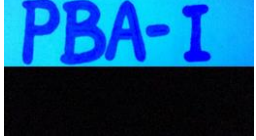
Common A4 paper			
PBA-OH	PBA-MeO	PBA-EtO	PBA-PrO
			
PBA-BuO		PBA	PBA-F
			
PBA-Cl	PBA-Br	PBA-I	
			

Fig. S43 Patterns written by PBA-AlkOs and PBA-Xs in acetone solutions (ca. 1.0 mol L⁻¹) on printing paper.

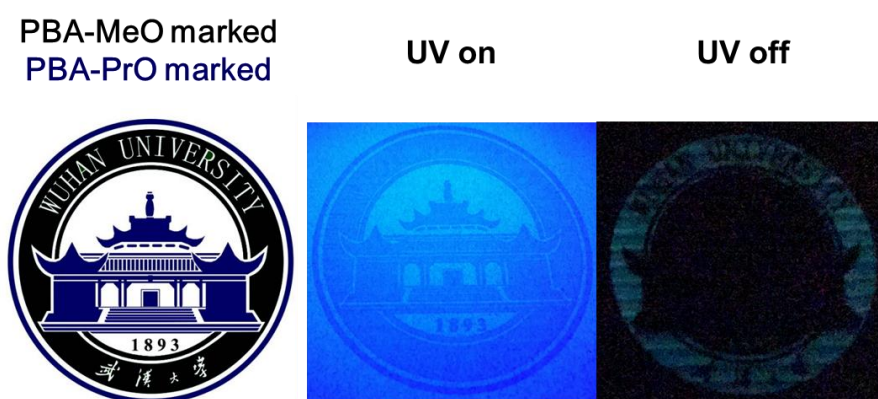


Fig. S44 Patterns printed with two phosphors.

10. Results of bio-toxicity determination. (Fig. 45, Table S6)

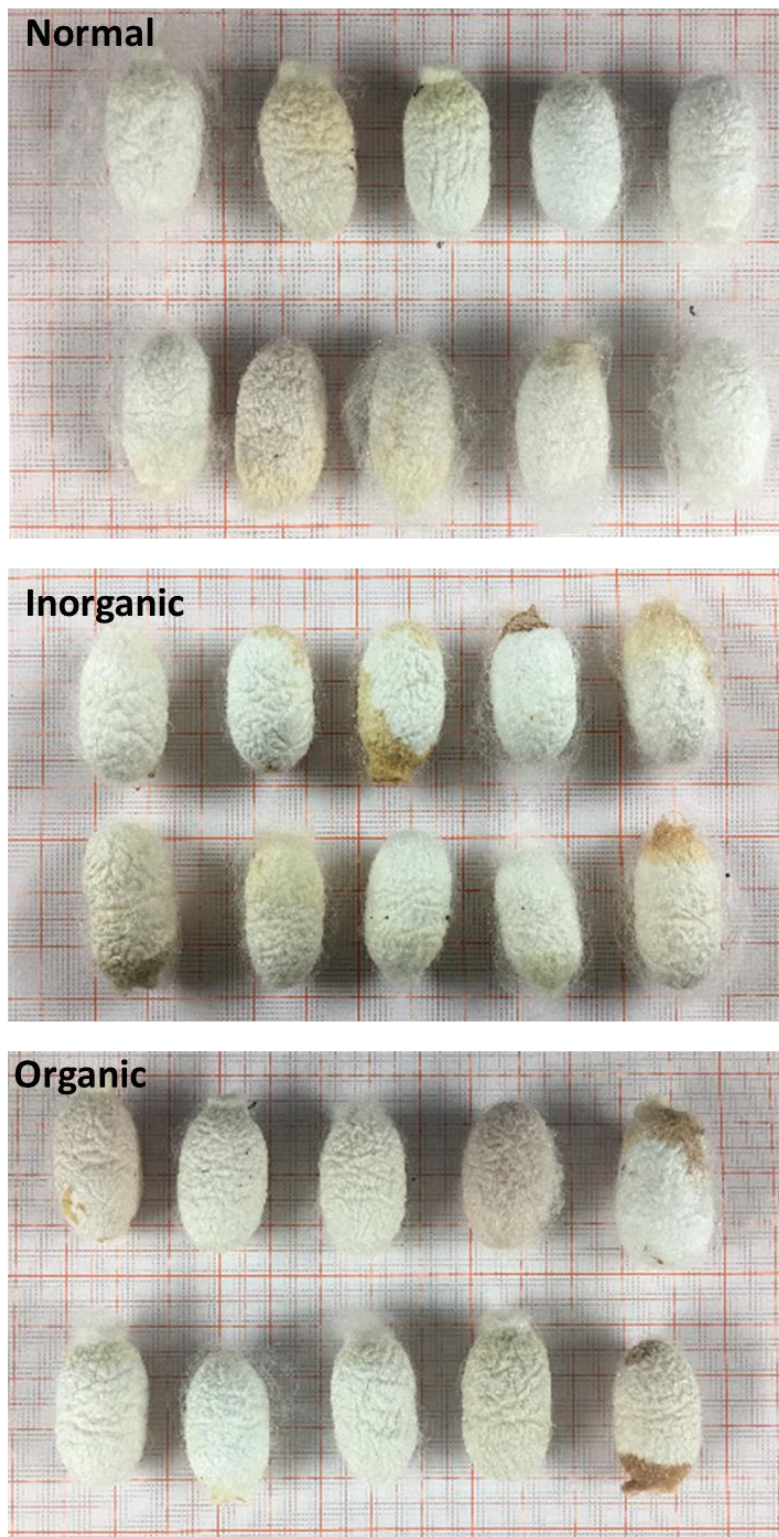


Fig. S45 Photographs of cocoons from silkworms fed with different diets.

Table S6 Mass distribution of different cocoons.

Unit: mg	①	②	③	④	⑤	⑥	⑦	⑧	⑨	⑩	Average Value
Normal	232	225	222	221	220	218	216	210	190	189	214.3
Inorganic Materials	212	197	189	186	185	184	178	174	166	165	183.6
Organic Materials	237	227	226	223	218	216	210	210	202	200	216.9

11. Materials

Boric acids were purchased from Soochiral Chemical Science & Technology Co., Ltd. Before use, they were hydrolyzed in boiling water (a small amount of acetone was added for PBA-Rs to prompt their dissolution) for 3 h and then filtered after being cooled in the air. tPBA-Rs were prepared through oil-water separation for 5 h, and then toluene was removed under reduced pressure. The substances were further kept in an electric vacuum drying oven at 80 °C for 2 h. All the compounds of PBA-AlkOs and tPBA-Rs were previously reported and characterizations were in consistency with the literatures^{6,7}. Tert-butyl 4-(4,4,5,5-tetramethyl-1,3,2-dioxaborolan-2-yl)benzoate (compound 32) was synthesized according to a literature procedure⁸. Inorganic phosphorescence materials (SrAl₂O₄:Eu²⁺,Dy³⁺, code: LM-001) were purchased from Kunyou Luminescence Co., Ltd.

12. Methods

Photoluminescence spectra were recorded on Hitachi F-4600. Powder X-ray diffraction patterns were recorded by Rigaku MiniFlex 600 with an X-ray source of Cu K α ($\lambda=1.5418$ Å) (25 °C, 40 KV, 15 mA). Single-crystal X-ray diffraction data were collected in a Bruker Smart Apex CCD diffractometer. The video and photographs of crystal luminance were taken by iPhone 6plus, while those of fast recrystallization were by Olympus IX71 research grade inverted microscope. The inkjet-printer used in this study was HP DeskJet 1110, and the printer cartridge was filled with PBA-MeO in mixed solvents of EtOH and water (v/v, 10:1).

The biotoxicity determination was carried out with *bombyx mori* silkworms in third instars (each group had 11 silkworms). The fresh mulberry leaves were sprayed with 1% concentration of PBA-MeO in MeOH (weight %) or inorganic suspension and fed the silkworms after been air-dried.

12. Computational details

Theoretical calculations were performed using Gaussian 09 program⁹. The ground state geometries were optimized with the B3LYP and 6-31G(d) basis sets. The excitation energies in singlet and triplet states were obtained with same methods, based on optimized configurations of monomer and dimers at ground state.

13. Reference

- 1 S. Kuno, T. Kanamori, Z. Yijing, H. Ohtani, H. Yuasa, *ChemPhotoChem*, 2017, **1**, 102.
- 2 Y. Shoji, Y. Iwabata, Q. Wang, D. Nemoto, A. Sakamoto, N. Tanaka, J. Seino, H. Nakai, T. Fukushima, *J. Am. Chem. Soc.*, 2017, **139**, 2728.
- 3 N. S. P. Bhuvanesh, J. H. Reibenspies, *Acta Crystallogr. Sect. E: Struct. Rep. Online*, 2005, **61**, 362.
- 4 M. A. Beckett, S. J. Coles, M. E. Light, L. Fischer, B. M. Stiefvater-Thomas, K. S. Varma, *Polyhedron*, 2006, **25**, 1011.
- 5 A. G. Avent, S. E. Lawrence, M. M. Meehan, T. G. Russell, T. R. Spalding, *Collect. Czech. Chem. Commun.*, 2002, **67**, 1051.
- 6 M. K. Smith and B. H. Northrop, *Chem. Mater.*, 2014, **26**, 3781.
- 7 K. Ishikawa, N. Kameta, M. Masuda, M. Asakawa and T. Shimizu, *Adv. Funct. Mater.*, 2014, **24**, 603.
- 8 T. C. Wang, W. Bury, D. A. Gomez-Gualdron, N. A. Vermeulen, J. E. Mondloch, P. Deria, K. Zhang, P. Z. Moghadam, A. A. Sarjeant, R. Q. Snurr, J. F. Stoddart, J. T. Hupp, O. K.

Farha, *J. Am. Chem. Soc.*, 2015, **137**, 3585.

- 9 M. J. Frisch, G. W. Trucks, H. B. Schlegel, G. E. Scuseria, M. A. Robb, J. R. Cheeseman, G. Scalmani, V. Barone, B. Mennucci, G. A. Petersson, H. Nakatsuji, M. Caricato, X. Li, H. P. Hratchian, A. F. Izmaylov, J. Bloino, G. Zheng, J. L. Sonnenberg, M. Hada, M. Ehara, K. Toyota, R. Fukuda, J. Hasegawa, M. Ishida, T. Nakajima, Y. Honda, O. Kitao, H. Nakai, T. Vreven, J. A. Montgomery, Jr., J. E. Peralta, F. Ogliaro, M. Bearpark, J. J. Heyd, E. Brothers, K. N. Kudin, V. N. Staroverov, T. Keith, R. Kobayashi, J. Normand, K. Raghavachari, A. Rendell, J. C. Burant, S. S. Iyengar, J. Tomasi, M. Cossi, N. Rega, J. M. Millam, M. Klene, J. E. Knox, J. B. Cross, V. Bakken, C. Adamo, J. Jaramillo, R. Gomperts, R. E. Stratmann, O. Yazyev, A. J. Austin, R. Cammi, C. Pomelli, J. W. Ochterski, R. L. Martin, K. Morokuma, V. G. Zakrzewski, G. A. Voth, P. Salvador, J. J. Dannenberg, S. Dapprich, A. D. Daniels, O. Farkas, J. B. Foresman, J. V. Ortiz, J. Cioslowski, and D. J. Fox, Gaussian, Inc., Wallingford CT, 2013.